Well-aligned arrays of vertically oriented ZnO nanowires electrodeposited on ITO-coated glass and their integration in dye sensitized solar cells

O. Lupan [a],[*],[1], V.M. Guérin [a], I.M. Tiginyanu [b], V.V. Ursaki [b], L. Chow [c], H. Heinrich [c], T. Pauporté [a],[*]

[a] Laboratoire d'Electrochimie, Chimie des Interfaces et Modélisation pour l'Energie (LECIME), UMR 7575 CNRS, École Nationale Supérieure de Chimie de Paris, Chimie-ParisTech, 11 rue P. et M. Curie, 75231 Paris Cedex 05, France
[b] Institute of Electronic Engineering and Nanotechnologies„ Institute of Applied Physics, Academy of Sciences of Moldova, MD-2028 Chisinau, Republic of Moldova
[c] Department of Physics, Department of Mechanical, Materials, and Aerospace Engineering, University of Central Florida, Orlando, FL 32816, USA

ARTICLE INFO

ABSTRACT

We report on the effects of post-growth hydrothermal treatment and thermal annealing on properties of vertically aligned ZnO nanowires arrays (NWs). The samples were electrochemically deposited (ECD) on indium–tin oxide (ITO)-coated glass substrates and subjected to post-growth hydrothermal treatment (HT) at 150 °C and, for the purpose of comparison, to conventional thermal annealing (CTA) in a furnace at 150, 400, and 600 °C in air. Sample characterization was realized using X-ray diffraction (XRD), SEM, TEM, selected-area electron diffraction (SAED) and photoluminescence (PL). Thermal annealing does not induce significant changes of morphology, but influences the structural and optical properties. At the same time we found that the HT induces more significant improvement of properties of ZnO nanowires arrays (ZnO NWs) on ITO. The results show that the ECD ZnO NWs are single-crystalline with hexagonal structure and c-axis perpendicular to ITO substrate. Only one peak at about 379 nm was observed in the photoluminescence spectra at room temperature which showed an intensity increase after hydrothermal treatment. This corresponds to the increase of the optical quality of ZnO NWs. The best optical quality for ZnO NWs was found after the hydrothermal treatments at 150 °C in our experiment. The high-quality electrodeposited NW layers have been used, after sensitization with the highly absorbing D149 dye, as a photoanode in dye sensitized solar cells (DSCs) and the impact of post-growth treatment of the nanowires on DSCs performances has been evaluated. The photocurrent of the solar cells increased significantly after HT or CTA at 150 °C leading to a maximum overall photovoltaic conversion efficiency (PCE) of 0.66% at 100 mW/cm², based on short-circuit photocurrent density, open-circuit voltage and fill factor of 3.283 mA/cm², 0.606 V and 33.3%, respectively. The obtained results are interesting in view of the low layer roughness and pave the way for implementation of high-quality electrodeposited ZnO NW arrays in DSCs fabrication.

1. Introduction

Zinc oxide (ZnO) is a wide and direct band gap (3.37 eV at room temperature) oxide semiconductor [1]. It has multiple potential applications in short-wavelength optoelectronic devices, solid-state display devices, solar cells, sensors, electrochromic windows, and exciting acoustic waves at microwave frequen-cies [2–7]. ZnO nanostructures such as nanowires (NWs) and nanorods (NRs) showed attractive characteristics for certain appli-cations [6–12]. This is because NWs/NRs show high aspect ratio, quantum confinement, and direct path for electrons promoting higher electron diffusion coefficient of ZnO nanowires arrays (ZnO NWs) with respect to nanoparticles films with multiple trap-ping/detrapping events occurring within grain boundaries [13–16]. The reported experimental results of transport properties on ZnO nanowires and nanorods are encouraging for device applications [17–19].

This is especially relevant because ZnO is considered as a strong competitor to GaN, which possesses the same wurtzite structure. Zinc oxide has a larger exciton binding energy (60 meV) than GaN (25 meV). In this way ZnO NWs are superior material for fabricat-ing low-threshold excitonic lasers and light-emitting diodes (LEDs)

* Corresponding authors. Tel.: +33 155426383; fax: +33 155426379.
   E-mail addresses: lupanoleg@yahoo.com, oleg-lupan@enscp.fr (O. Lupan),
thierry-pauporte@chimie-paristech.fr (T. Pauporté).
   [1] On leave from Department of Microelectronics and Semiconductor Devices, Technical University of Moldova, 168 Stefan cel Mare Blvd., MD-2004 Chisinau, Republic of Moldova.

[20,21]. Optical UV lasing and LED have been demonstrated either at low or high temperatures [20,21].

Aligned ZnO NWs arrays are considered as a competitor to TiO$_2$-based dye-sensitized (photoelectrochemical, quasisolid, and solid-state) solar cells (DSCs) owing to the unsuccessful development of vertical single-crystalline TiO$_2$ NWs on the transparent conducting oxide substrate [22]. Zinc oxide has approximately the same energy band gap and electron affinity as titanium dioxide, and ZnO DSCs built using ZnO nanoparticles (NP) have shown the second highest efficiencies (up to 6.5%) after TiO$_2$ [23–25]. For example Law et al. [16] found that the electron diffusion coefficient of ZnO NWs is several hundred times larger than that of ZnO or TiO$_2$ NP films. With aligned ZnO NWs several problems can be solved in devices based on the nanoporous materials, which rely on the trap-limited diffusion for electron transport, a slow mechanism that limits electron extraction efficiency [26,27]. It is expected that a more direct conduction pathway from the point of electron–hole pair generation to the collection electrode would significantly improve the electron transport efficiency [26,28].

Different techniques such as vapor deposition, pulsed laser deposition, molecular beam epitaxy, metal organic chemical vapor deposition (MOCVD), sputtering, electron beam evaporation, spray pyrolysis, sol–gel processing, chemical, and electrochemical deposition have been employed to fabricate ZnO NWs/NRs [10,29–32]. For example, several reported methods permit to grow ZnO nanowires nearly vertically from the substrate [16,25,32–37]. Among numerous deposition techniques, electrochemical deposition (ECD) has become attractive for fabricating ZnO NWs/NRs owing its simplicity, and less onerous, widely used in industry [14,32,38], cost-efficiency, large-area deposition and high-quality NWs/NRs can be grown at relative low synthesis temperatures [32–34]. Therefore, an accurate knowledge of the structural, morphological and optical properties of ZnO is essential for the design and analysis of various devices. Despite of multiple possible methods to fabricate ZnO nanomaterials, according to previous reports the properties of ZnO NWs are strongly dependent on the fabrication conditions and the preparation methods, e.g. substrate temperature, substrate material and subsequent annealing treatment [30,37–42].

Above all, the selection of substrate is very important for the growth of arrays of high-quality ZnO NWs, because the matching in lattice parameters and crystal structure between the NWs and substrate strongly affects the crystal growth behavior and quality [43]. Indium–tin-oxide (ITO)-coated glass substrate has many excellent properties, such as electrical conductivity and optical transparency, high vis–NIR light transmission, uniform transmission homogeneity and reflection in the infrared range [40–41,44–45]. The lattice mismatch is small (3%) between the neighboring oxygen–oxygen (O–O) distance on the close-packed ITO (1 1 1) and ZnO (0 0 0 1) planes [46], and O dangling bonds on the ITO layer surface, thus it improves the initial nucleation and the subsequent growth of high-quality ZnO NWs arrays on ITO substrate. Up to date, a few studies have reported on the growth of the high optical quality of aligned ZnO NWs arrays on ITO glass substrate [40,47] with promising applications in solar cells. Such structure based on aligned ZnO NWs/ITO is very attractive for the dye-sensitized solar cells.

In this report, aligned ZnO NWs have been fabricated by using ECD on ITO at low temperature. Then ZnO NWs were treated using thermal and hydrothermal techniques with subsequent characterization of structural and optical properties. The influence of the ITO buffer layer on the structural and photoluminescence properties of ZnO NWs is reported. Note that zinc oxide nanowire architecture provides an open structure for filling with a hole transport material. The present paper is the first report on the use of cost effective electrodeposited NW arrays for DSCs fabrication.

2. Experimental

2.1. Electrochemical deposition of ZnO nanowires arrays

Well-aligned ZnO nanowires arrays (ZnO NWs) were grown by the electrochemical deposition (ECD) method from a 0.2 mM ZnCl$_2$ (Merck, 99%) aqueous solution maintained at 85 °C as reported before [32,39,48]. For supporting electrolyte, 0.1 M of potassium chloride (KCl) (Fluka 98%) was employed to ensure a good electrical conductivity in the aqueous solution (Milli-Q quality water). The ZnO NWs were grown on the conductive indium-doped tin oxide (ITO) film on a glass substrate with a sheet resistance of 15 Ω/□. Electrodeposition was carried out potentiostatically at −1.05 V using an Autolab PGSTAT30 potentiostat/galvanostat and with rotation of working electrode (WE) (with constant speed of ω = 300 rotations/min (rpm)). The potentiostat was monitored by the AutoLab software. The pH of the solutions was initially 5.5. The three-electrode electrochemical cell was mounted in a thermoregulated bath and the temperature was fixed at 85 °C with an uncertainty of ±0.2 °C. The electrolyte was saturated with pure oxygen by bubbling for 45 min prior to start the electrolysis and continuously during of the growth process. The growing process ended in 9000 s when the total passed/exchanged electrical charge reached 14.0 C/cm^2.

Fig. 1a is a typical current–voltage (I–V) curve of the real ITO–electrolyte interface recorded upon a first voltammetry scan started at the rest potential on the bare ITO electrode. The observed
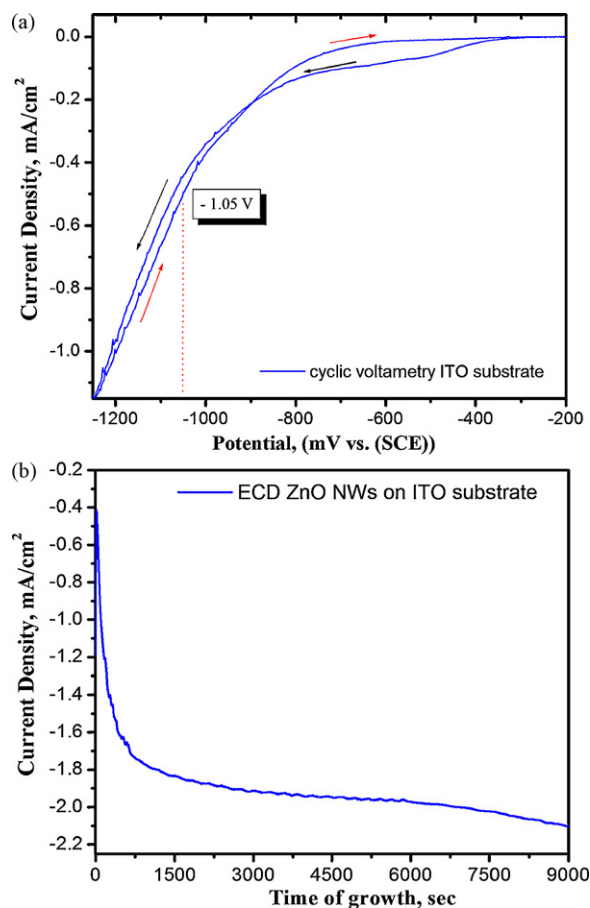

Fig. 1. (a) Cyclic-voltammetry J–V characteristic of rotating ITO/glass electrode for the solution containing 0.2 mM ZnCl$_2$ + 0.1 KCl (pH 5.5) under oxygen bubbling. (b) Variation of current density with time during of ECD of ZnO NWs on ITO substrate at 85 °C, E = −1.05 V/SCE with rotating working electrode (ω = 300 rpm).

cathodic wave can be assigned to the electrochemical reduction of molecular oxygen and the hysteresis is due to the covering of the ITO surface by ZnO upon the first scan [49]. From the figure, a deposition potential of 1.05 V was chosen for the synthesis of the layers. Fig. 1(b) displays the current transient recorded at that potential upon nanowire deposition on ITO substrate at 85 °C, with a rotation speed of 300 rpm. The illustrated curve confirms that the ECD ZnO NWs are good electrical conductors, because the current density collected at the electrode is kept at about −1.85 mA/cm^2 after 1000 s of growth. Fundamental physicochemical properties of cathodic ZnO synthesis in an aqueous zinc chloride solution of [ZnCl$_2$] = 0.2 mM have been described previously [32,39,48].

After electrodeposition, ZnO NWs/ITO were thoroughly and carefully rinsed with DI water to remove chloride salts and unreacted products from the surface and dried under a moderate air flux. The hydrothermal treatment (HT) was carried out at 150 °C in a stainless steel autoclave. A 100 mL Teflon inner liner was used and the sample was maintained at about 3 cm above the water surface level to avoid direct contact between ZnO and water. The HT treatment was compared to conventional CTA at 150 °C in air for 1 or 12 h. Annealing at 400 and 600 °C in air for 1 h were also investigated.

2.2. ZnO nanowire films and solar cell characterizations

Phase identification of the ECD ZnO NRs/NWs on ITO was done with a X-ray diffractometer Siemens D5000 operated with 40 kV and 45 mA using the Cu Kα radiation with λ = 1.5406 Å and a rotating sample holder. The morphologies of the samples were investigated with a high resolution Ultra 55 Zeiss FEG scanning electron microscope at an acceleration voltage of 10 kV. Energy dispersive X-ray spectroscopy (EDX) analyses were realized with a Bruker Li-drift silicon detector. A TEM sample was prepared by a direct contact technique of the sample with a clean Si wafer to transfer nanowires and gently rub a few times [3,30,48]. Transmission electron microscopy (TEM) and selected-area electron diffraction (SAED) measurements were performed on a FEI Tecnai F30 STEM operated at an accelerating voltage of 300 kV.

Raman scattering was measured at room temperature with a Horiba Jobin Yvon LabRam IR system in a backscattering configuration. A 632.8 nm line of a He–Ne laser was used for off-resonance excitation with less than 4 mW power at the sample. The instrument was calibrated using silicon and a naphthalene standard. The continuous wave (cw) photoluminescence (PL) was excited by the 325 nm line of a He–Cd Melles Griot laser. The emitted light was collected by using a lens and was analyzed with a double spectrometer ensuring a spectral resolution better than 0.5 meV. The signal was detected by a photomultiplier working in the photon counting mode. The laser power for the PL excitation was about 20 mW. The samples were mounted on the cold station of a LTS-22-C-330 optical cryogenic system.

For solar cell preparation, aligned 4.5 μm long ZnO NWs prepared by electrodeposition were dried at 85 °C for 10 min and then sensitized by D149 (Chemicrea), a high performance indoline dye [50]. A reflecting film of Pt deposited by evaporation on a glass substrate was used as a counter-electrode. The liquid electrolyte was composed of 0.6 M tetrabutylamonium iodide (Sigma); 0.01 M LiI (Fluka) and 0.05 M I$_2$ (Aldrich). The active area of the cell was delimited with a metallic mask of 0.07 cm^2. I–V characterizations were made in air using a calibrated solar simulator (Abet Technologies) under AM1.5 illumination and light intensity of 100 mW/cm^2. Current–voltage (J–V) characteristics of solar cells were recorded by a Keithley 2400 digital multi-meter using 0.01 V/s voltage ramp rate.
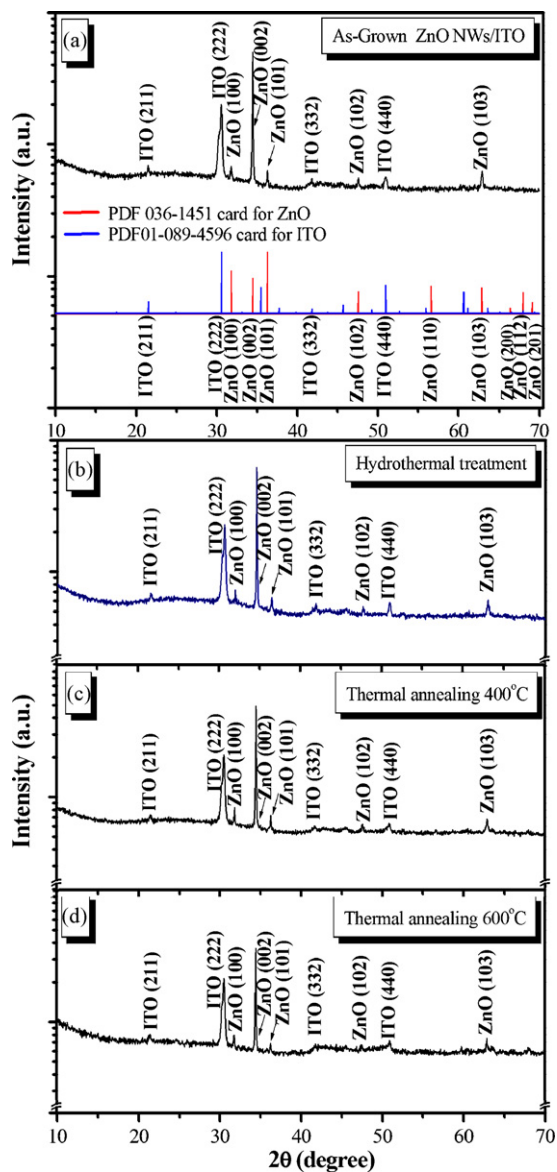

Fig. 2. XRD spectra of ZnO NWs grown by electrochemical method at 85 °C on ITO substrate: (a) as-grown; ITO substrate peaks are marked by a blue line and ZnO by red line peaks according to JCPDS; (b) hydrothermally treated at 150 °C for 12 h; (c) thermally annealed at 400 °C for 1 h; (d) thermal annealed at 600 °C for 1 h. (For interpretation of the references to color in this figure legend, the reader is referred to the web version of the article.)

3. Results and discussion

3.1. Structural and morphological characterization of ZnO nanowire arrays

Fig. 2 shows the effects of the post-growth hydrothermal treatment and conventional thermal annealing temperature on the crystallinity of the ECD ZnO NWs/ITO. All XRD peaks (Fig. 2) are assigned to ITO-coated glass substrates according to PDF 01-089-4596 card or to ZnO based on PDF 036-1451. It can be seen that electrodeposited ZnO NWs show a sharp XRD reflection peak detected at ∼34.4°, suggesting a preferential growth along the c-axis normal to the ITO substrate. The intensity of the peaks relative to the background demonstrates high purity of the hexagonal ZnO phase and good crystallinity of the samples. The lattice constants a and c were determined as 0.3251 nm, 0.5205 nm using the follow-

ing equation [30,48]:

$$\frac{1}{d^2_{(hkl)}} = \frac{4}{3}\left(\frac{h^2 + hk + k^2}{a^2}\right) + \frac{l^2}{c^2}. \tag{1}$$

The lattice parameter $d(002)$ in the un-stressed ZnO bulk is about 2.602 Å, and the $d(002)$ value of as-grown ECD ZnO on ITO is 2.601 and 2.600 Å after hydrothermal treatment and thermal annealing at 400 or 600 °C.

All observed Bragg reflections are consistent with the Wurtzite $P6_3mc$ space group. The intensity reaches the maximum value after hydrothermal treatment at 150 °C for 12 h (Fig. 2b). The small full width at half-maximum (FWHM) values (0.125° and 0.093° for the as-grown and hydrothermally treated samples, respectively) reveals that the ZnO is of high crystalline quality. The FWHM values of (002) peaks are 0.093° for the samples after thermal annealing at 400 and 600 °C.

The texture coefficient for the (002) orientation is estimated to be about 3.5 from the following relation [30,32,48]:

$$TC_{(0\,02)} = \frac{I_{(002)}/I^0_{(002)}}{(1/N)\sum I_{(hkl)}/I^0_{(hkl)}}, \tag{2}$$

where N is the number of diffraction peaks, and $I_{(hkl)}$ and $I^0_{(hkl)}$ are the measured and corresponding recorded intensities according to the JCPDS 036-1451 card. The high $TC_{(002)}$ value shows that the wires are very well-textured with the c-axis perpendicular to the substrate. As described elsewhere, the growth of the more initially inclined wires is impeded whereas it is favored for the more vertically oriented ones [32].

On SEM images (Fig. 3) the layer appears to be homogeneous and uniform. The nanowires are vertically oriented and well-aligned. The average size is ∼160–220 nm in width and ∼4–5 μm in length. Their density is low at 4–5 NWs per μm². There is an excellent adherence and connection between ZnO NWs and ITO substrate (Fig. 3, inset).

Transmission electron microscopy (TEM) was employed to characterize the as-synthesized ZnO NWs and to investigate the effect of annealing on its structure. The TEM image in Fig. 4 shows the crystal structure of the individual ZnO NW and their average radii of about 75–100 nm. TEM images show also that the diameter size is homogeneous and does not vary significantly along the wire length.

HRTEM and SAED in Fig. 4b demonstrate the high-quality of the as-grown sample at the atomic scale. By controlling accurately the deposition regimes within the optimum range of the energetically stable state, ZnO NWs arrays grow with a c-axis orientation. These HRTEM data are corroborated with the results of XRD measurement in our work. It is suggested that for ZnO (002) orientation, the surface energy reaches a minimum and the growth orientation develops into one crystallographic direction of the lowest surface energy [48,51]. The (002) texture of the zinc oxide NW must form in an effective equilibrium state where enough surface mobility is given to impinging atoms under a certain deposition condition [48,52]. The HRTEM images also illustrate that the surface of the as-grown wires appear crystallized with the absence of any amorphous layer.

The present study illustrates the beneficial effect of reactive treatment by air oxygen and water vapor for enhancing ZnO NWs structural and optical properties. Water vapor acts more efficiently than oxygen to reduce structural defects. According to our studies [53] the post-growth hydrothermal treatment suggests that ZnO recrystallization can occur locally. Water vapor may also react with atoms in excess or vacancies near the surface. For instance, using a mass spectrometer, Hasebe et al. [54] have shown that the excess of zinc at zinc oxide surfaces can react with water vapor to produce
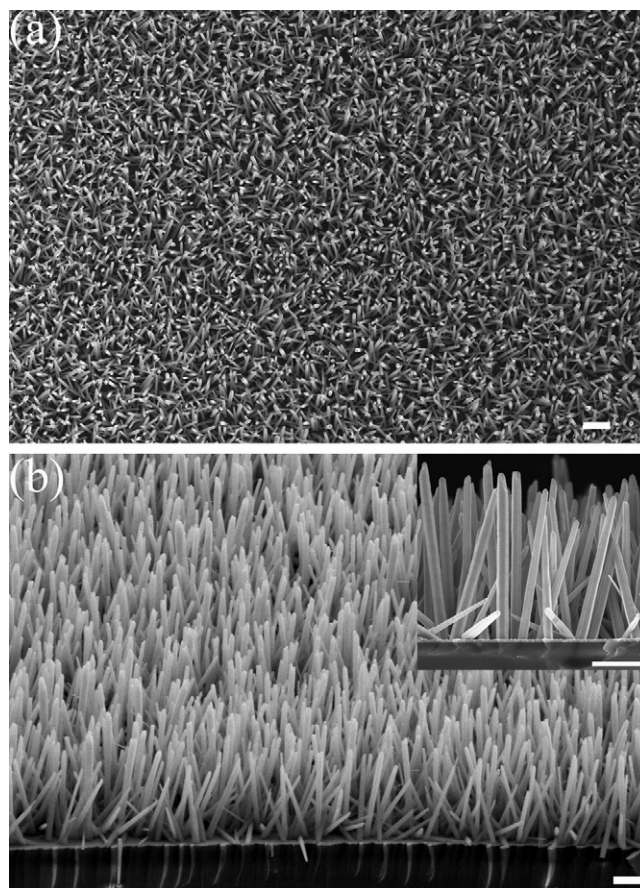

Fig. 3. SEM images of ECD aligned ZnO nanowire arrays on ITO glass: (a) plan view; (b) a tilted-view (65°), insert is a cross-sectional view of ZnO NWs forming arrays. Scale bar is 1 μm.

ZnO and hydrogen:

$$Zn + H_2O \rightarrow ZnO(s) + H_2(g) \tag{3}$$

It seems in our hydrothermal treatment in an autoclave that various surface defects reacted with adsorbed water molecules, which led to an improved ZnO surface. In this way, a higher PL emission intensity is obtained. However, the duration of hydrothermal treatment and water pressure in an autoclave are important parameters due to consumption of Zn_i and other point defects by water vapor. This would lead to a significant decrease in the visible PL emission.

3.2. Micro-Raman scattering

Raman measurements are useful for the purpose of exploring the material quality, the phase and purity, in order to understand transport properties and phonon interaction with the free carriers, which determine device performances [10,48]. The point group of ZnO is C_{6v}, and there exist 12 degrees of freedom since there are 4 atoms per primitive cell. Therefore there are nine optical phonon modes and three acoustic phonon modes. Phonon modes E_2 (low and high frequency), A_1 [(TO) transverse optical and (LO) longitudinal optical] and E_1 (TO and LO) are expected all being Raman active. According to group theory, the optical mode at the Γ point of the Brillouin zone can be expressed by [48]:

$$\Gamma_{opt} = 1A_1 + 2B_1 + 1E_1 + 2E_2 \tag{4}$$

A_1, E_1, and E_2 are Raman active modes, except the silent mode B_1. Fig. 5 shows the effect of various post-growth treatments on sample Raman spectra measured in backscattering geometry. The Raman
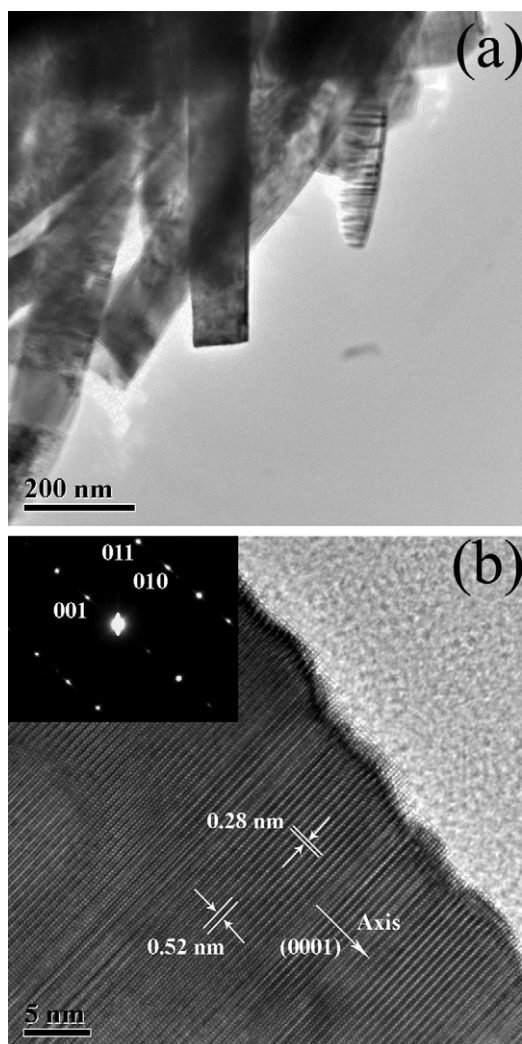
Fig. 4. (a) TEM of as-electrodeposited ZnO nanowires on ITO substrate showing a general view; (b) HRTEM image showing individual nanowire with [0 0 2] growth direction. Inset shows selected electron diffraction patterns (SAED). Both SAED and HRTEM images are indicative of high crystalline quality for most of the ECD ZnO NWs.
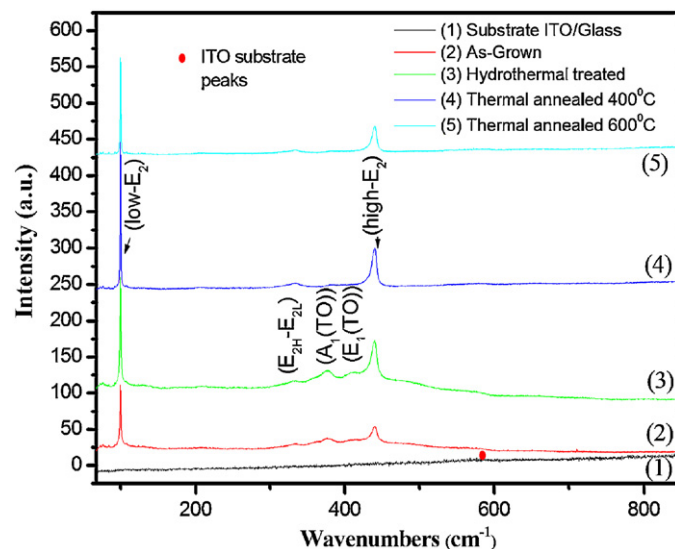

Fig. 5. Raman spectra for as-grown, hydrothermal treated at 150 °C and thermal annealed ZnO NWs on ITO substrate. Curve 1 shows Raman spectra from the ITO substrate.

spectrum from the ITO substrate itself is presented for reference (Fig. 5, curve 1). It can be observed on zoom-in (not shown) that the broad peaks at 106, 573, and 635 cm^{-1} are from ITO substrate as-received before ECD process and can be found in all spectra. In Fig. 5, the E_2 optical mode is observed as dominant peaks at 100 and 438 cm^{-1}, which are commonly detected in the wurtzite structure ZnO [10,48]. The better observation of the E_2(high) mode on annealed samples indicates that the crystalline quality of the ZnO thin films is improved with annealing. Especially, the Raman spectrum of the ZnO film annealed at 400 °C demonstrates the good quality of the wurtzite crystal structure in the produced material.

All three treated samples exhibit similar scattering peaks, indicating that they have identical crystal structures as confirmed by XRD. However, hydrothermal treated ZnO NWs have also the A_1(TO) and E_1(TO) modes at 381 and 411 cm^{-1}, respectively, and the high order Raman peaks at 316 cm^{-1} (LO-B_1) and 336 cm^{-1} (TO-E_2). The E_2(high) peak position is at 438 cm^{-1} for as-grown sample, CTA and hydrothermal treated at 150 °C for 12 h in autoclave. Sample after CTA 150 °C for 1 h has similar characteristics (not shown) as HT sample.

The peak positions of the optical phonon modes were in good agreement with the results reported by Calleja and Cardona [55]. The FWHM of the peak corresponding to low-E_2 (100 cm^{-1}) mode from hydrothermally treated and thermally annealed samples is about 1.1 cm^{-1}, which is comparable to values reported for high-quality ZnO bulk crystals [48]. Also, the position of the E_2 (high) peak of annealed samples corresponds to the phonon of a bulk ZnO crystal [48] indicating a strain-free state of the electrodeposited ZnO.

3.3. Photoluminescence characterizations

PL is a well-known powerful technique to probe the quality of ZnO, especially the presence of deep intrinsic defects [10,39]. The PL spectrum of the as-prepared sample (Fig. 6a) consists of a broad asymmetric near bandgap band with a pronounced tail in the region of low photon energies. A similar shape of the near bandgap luminescence has been previously observed in highly doped ZnO samples grown by different methods [56–59]. It was previously shown that this PL band is due to direct transitions of electrons between the conduction to valence band tails [56,57]. The broadening of the PL band involved can be accounted for by the broadening of the band edges due to potential fluctuations induced by the high concentration of intrinsic defects or impurities. The width of the band tails, and the dependence of the full width at half-maximum (FWHM) of the PL band on carrier concentration, can be calculated using the model for broadening of impurity bands in heavily doped semiconductors developed by Morgan [60].

The hydrothermal treatment of the sample leads to the narrowing of the PL band and the increase in the intensity by an order of magnitude (Fig. 6b). One should note that annealing in air in the temperature interval 150–400 °C also results in the increase of the PL intensity (Fig. 6c and d). However, this increase is by a factor of less than 3 as compared to the as-prepared sample.

The FWHM of the PL band in the as-prepared sample as well as of samples subjected to different treatments as a function of temperature is shown in Fig. 7a. By using the established dependence of the FWHM of the PL band on carrier concentration [56–58], one can estimate the electron concentration in our samples as a function of temperature. Fig. 7b presents the Arrhenius plot of the free electron concentration deduced for the FWHM of the PL band according to the Morgan model. One should note that annealing of the sample at 400 °C leads to the change of the shape of the near bandgap luminescence spectrum, revealing two bands with the maxima at 3.30 and 3.33 eV at low temperature (Fig. 6d). The band at 3.30 eV has a LO phonon replica at around 3.23 eV. Therefore, the Morgan model
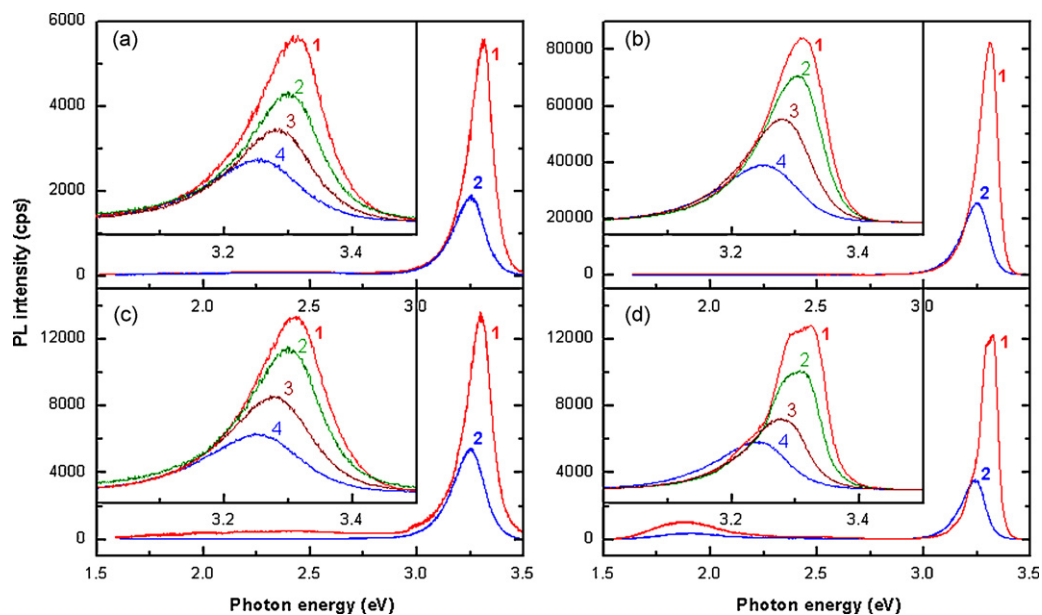
Fig. 6. Near bandgap PL spectrum of the as-prepared sample with ZnO NWs on ITO substrate (a); the sample subjected to the HT treatment (b); the sample annealed in air at 150 °C (c), and 400 °C (d). The spectra are measured at $T = 10$ K (curve 1) and $T = 300$ K (curve 2). Inset are the spectra measured in the near bandgap spectral range at $T = 10$ K (curve 1), $T = 100$ K (curve 2), $T = 200$ K (curve 3), and $T = 300$ K (curve 4).
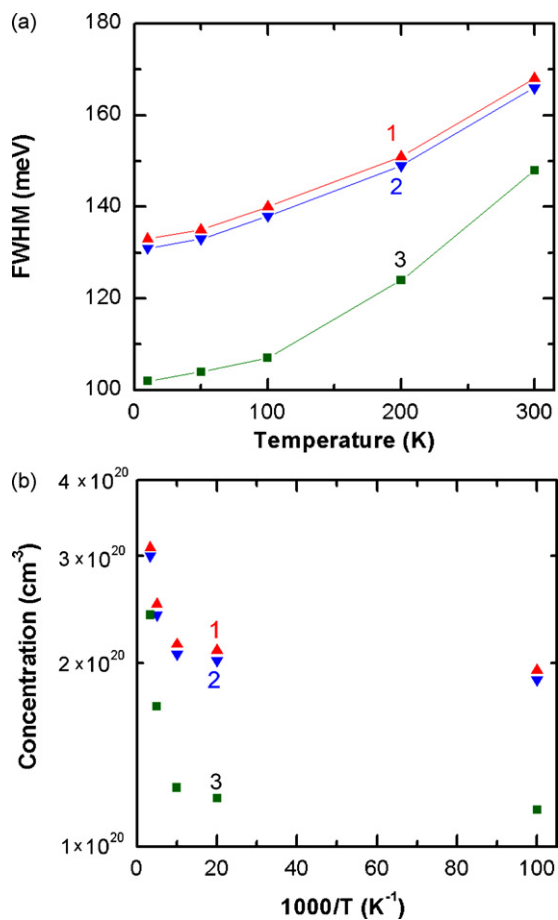

Fig. 7. FWHM of the near bandgap PL band (a); and free electron concentration deduced from the FWHM (b) as a function of temperature for the as-prepared sample (1); the sample annealed at 150 °C (2), and the sample subjected to the HT treatment (3).

cannot be applied to determine the free carrier concentration in this sample.

One can see from Fig. 7b that the HT treatments result in the decrease of the free carrier concentration at low temperatures from 2×10^{20} to 1×10^{20} cm^{-3}. As concerns the microscopic origin of the impurity determining the free carrier concentration and the broadening of the near bandgap PL band, one can assume that it is related to defects. However, the contribution of the deviation from stoichiometry cannot be withdrawn. Oxygen vacancies and zinc interstitials are the most probable donor-type intrinsic defects [61–62]. Oxygen vacancy is a deep donor, while zinc interstitial is a shallow one [61]. Thus, Zn_i defects can contribute to the high electron concentration.

One should note that annealing of samples in air at temperatures above 400 °C leads to a decrease of the near bandgap PL intensity. Therefore, the near bandgap PL intensity of samples annealed at any temperatures in air is lower as compared to the samples subjected to HT treatment. Another observation is the emergence of two PL bands at 1.85 and 2.55 eV in the visible spectral range in samples subjected to thermal treatment in air. The intensity of this emission increases with increasing the annealing temperature. At the same time, no visible emission was observed in samples subjected to HT treatment. It is known that the visible emission in ZnO is associated with various structural defects. Therefore, the PL analysis demonstrates the very high-quality and the near stoichiometry of the ZnO NWs subjected to HT treatment. The improvement of the ZnO NWs quality induced by HT treatment facilitates also the charge transfer as shown in the following section of the paper.

3.4. Applications to dye-sensitized solar cells

According to previous reports a superior device efficiency is anticipated by replacing the nanoparticulate film with a vertical single-crystalline nanowire array for enhancing the electron transport rate [22,28]. It was reported that the ZnO nanowires exhibit significantly higher electron mobility compared to both TiO$_2$ and ZnO nanoparticle films [42] and for instance Law et al. found that the electron diffusion coefficient of ZnO NWs is several hundred times larger than that of ZnO or TiO$_2$ NP films [16]. The development
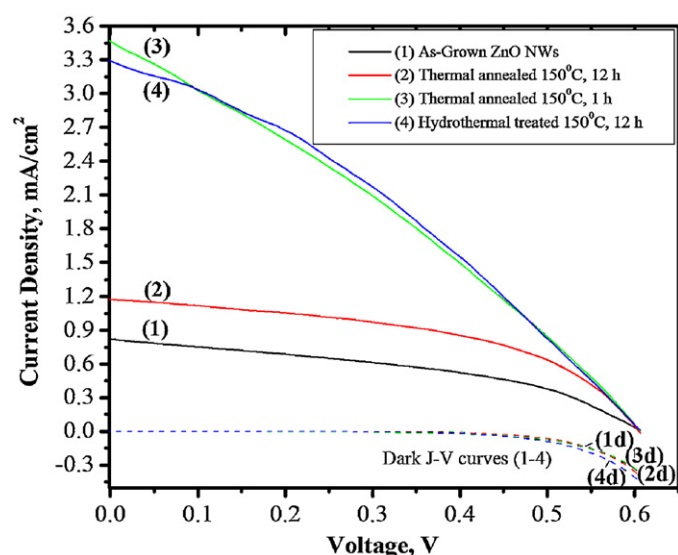
Fig. 8. J–V characteristics (full line) for 4.5 μm long ZnO nanowire arrays electrodeposited on ITO electrode (0.07 cm^2) sensitized with D149 (simulated AM1.5G illumination with intensity 100 mW/cm^2). Dark J–V characteristics (dashed line).

of vertical single-crystalline ZnO NW array DSCs on the transparent conducting oxide substrate have been demonstrated up to now [12,16,25,35,63].

The high-quality ZnO NWs arrays described in the previous section have been used after dye sensitization as a photoanode in dye-sensitized solar cells. The D149 indoline dye was chosen due to its high molecular extinction coefficient (measured at 78 000 M^{-1} cm^{-1} in acetic acid) and its good compatibility with ZnO in part due to a reduced complexing properties for zinc ions [50]. It is important to note that depending on the rates of the diffusion of the dye into the nanostructure, adsorption of the dye, dissolution of Zn surface ions and formation of aggregates in the pores of the film, the outer part of the electrode may be in the process of forming aggregates when the two first mentioned processes occur close to the back contact. Thus, it is difficult to avoid dye aggregation completely and the dye treatment has to be optimized for a given film thickness in order to obtain the highest possible solar cell efficiency.

The relationship between I–V curves and different types of treatment is illustrated in Fig. 8, in which we can see that short-circuit photocurrents increase markedly for treated samples and espe-

cially for those treated at 150 °C. The characteristics of the curves are summarized in Table 1 expressed in terms of open-circuit voltage (V_{oc}), short-circuit current (I_{sc}), fill factor (FF) and overall solar-to-electric energy conversion efficiencies (η).

The best efficiencies are found for the sample treated at 150 °C either by HT or by CTA. However, the later the treatment must be rather short, 1 h, since the efficiency decrease after a 12 h annealing. It is probable that the better performance is due to an improvement of the wire surface quality that favors the dye anchoring and then the charge transfer upon functioning. We have shown that the treatments also improve the bulk quality and may have an influence on the charge transfer to the back contact. The low efficiency is mainly due to a low fill factor which most likely results from back reaction between photoexcited electrons in the zinc oxide nanowires and tri-iodide ions in the filling electrolyte. The back reaction is evident in the low value of the shunt resistance, $R_{sh} = (dV/dI)_{v=0}$, in the I–V characteristics recorded under illumination, see Fig. 8a. Annealing at a temperature higher than 150 °C is detrimental for the cell performances due to the decrease in ITO substrate conductivity according to our experimental observations.

Table 1 also compares the performances of the cells based on the electrodeposited 4.5 μm long wires with the literature data. The present results are much better than those reported in Ref. [64] in which the same dye was used. We can also note that the electrodeposited wires are more efficient for light conversion than the other wires of similar length produced by other solution growth techniques. This is probably due to the remarkable quality of their bulk and surface and a very good electrical contact between the wires and the substrate inferred to the growth method. In Ref. [65] the slightly better performance is due to a higher FF. The best results in Refs. [16,66] have been achieved by using dense arrays of ZnO NWs with length longer than 11 μm.

Previous reports ascribed the low current density of nanorod-based DSCs to the small surface area of the nanorod array with low dye loading and light harvesting [25,66]. In the present work the layer roughness is low at 14–15 but the light harvesting has been improved by using a highly absorbing organic dye and a reflecting Pt counter-electrode. The short-circuit current density is remarkably high in view of this low layer roughness. Interface recombination and band reaction loss in ZnO NWs-based DSCs is mostly due to the uncovered oxide surface (with no dye molecule anchored on), where oxide contacts (substrate and NWs) with electrolyte closely and thus increases probability of charge reaction between the electrons in oxide and tri-iodide in the electrolyte [66].

It looks that the surface area and back reaction limit the present ZnO NWs-based DSCs solar cells, and further work is required

Table 1
Comparison of the performance parameters extracted from I–V characteristics of ZnO nanowires/ITO electrodes with 4.5 μm in length under 100 mW/m^2 illumination using a standard electrolyte solution.

Sample 4.5 μm long NWs	Dye and residence time	V_{OC}, V	J_{SC}, mA/cm^2	FF	R_{serie}, Ω cm^2	R_{shunt}, Ω cm^2	PCE η, %
As-grown	D149	0.584	0.812	41.5	309.7	1303.6	0.20
Hydrothermal treated at 150 °C, 12 h	D149	0.606	3.28	33.3	132.1	381.6	0.66
Thermal annealed at 150 °C, 1 h	D149	0.605	3.44	30.6	129.7	305.3	0.64
Thermal annealed at 150 °C, 12 h	D149	0.606	1.17	49.2	175.6	1840.7	0.35
Thermal annealed at 400 °C, 1 h	D149	0.553	2.08	34.8	174.6	559.4	0.40
Thermal annealed at 600 °C, 1 h	D149	0.534	0.774	40.6	326.7	2230.2	0.17
Results from literature							
[64] 8 μm in length NWs	D149	0.47	0.71	–	–	–	0.088
[67] 8 μm in length NWs	N719, 30 min	0.67	1.3	32.0	–	800	0.3
[68] 5 μm in length NRs	N3, 6 h	0.34	0.49	45.0	–	–	0.32
[69] 5.5 μm in length NWs	Mercurochrome, 20 min	0.44	2.15	47.0	–	–	0.45
[25] 10 μm in length NWs	N719d, 30 min	0.74	1.62	38.0	–	–	0.5
[26] 3.2 μm in length nanotips	N719, 1 h	0.662	2.040	41.0	124.0	–	0.55
[65] 5.5 μm in length NWs	Mercurochrome	0.50	3.4	49.0	–	–	0.84
[66] 11 μm in length NW	N719, 1 h	0.63	4.5	36.0	–	–	1.0
[16] 20–25 μm in length ZnO NWs array with a 10–15 nm ZnO film seed	N719, 1 h	0.61–0.71	5.30–5.85	36.0–38.0	–	–	1.2

to obtain higher density of longer ZnO NWs. The engineering of semiconductor NWs design morphology can open possibilities for improved charge transport and easy filling with solid hole conductors. The use of a simplified geometry is also clearly a means for a better understanding of device physics.

4. Conclusions

Aligned ZnO nanowire arrays were grown on ITO substrates by the electrochemical method. The effects of low temperature hydrothermal treatment and thermal annealing treatment at 150, 400 and 600 °C on the crystallinity, Raman spectra and photoluminescence of ZnO NWs electrodeposited on ITO substrates were analyzed.

This study demonstrates that the hydrothermal treatment has the most beneficial effect indicated by the increase in (0 0 2) diffraction intensity of XRD pattern and the highest luminescence intensity. The physical parameters of the electrodeposited ZnO films are improved due to the annealing of intrinsic and extrinsic defects.

The ZnO nanowires used in this study show suitable properties for further studies with respect to solar energy conversion applications. The improvement in the overall solar cell efficiency from 0.2% to 0.66% in the present work originates from a controlled dye sensitization procedure (avoiding dye aggregation) and from the new method (the exclusion of organic additives probably leads to better interfacial kinetics). The properties of the ECD ZnO NWs films prove to be good which makes this method promising for future applications.

Acknowledgements

References

[1] H.E. Brown, Zinc Oxide Rediscovered, The New Jersey Zinc Company, New York, 1957.
[2] O. Lupan, S. Shishiyanu, V. Ursaki, H. Khallaf, L. Chow, T. Shishiyanu, V. Sontea, E. Monaico, S. Railean, Synthesis of nanostructured Al-doped zinc oxide films on Si for solar cells applications, Sol. Energy Mater. Sol. Cells 93 (2009) 1417.
[3] O. Lupan, L. Chow, G. Chai, L. Chernyak, O. Lopatiuk-Tirpak, H. Heinrich, Focused-ion-beam fabrication of ZnO nanorod-based UV photodetector using the in-situ lift-out technique, Phys. Stat. Sol. A 205 (2008) 2673.
[4] G. Chai, O. Lupan, L. Chow, H. Heinrich, Crossed zinc oxide nanorods for ultraviolet radiation detection, Sens. Actuators A: Phys. 150 (2009) 184.
[5] G.C. Yi, C.R. Wang, W.I. Park, ZnO nanorods: synthesis, characterization and applications, Semicond. Sci. Technol. 20 (2005) S22–S34.
[6] (a) O. Lupan, G. Chai, L. Chow, A single ZnO tetrapod-based sensor, Sens. Actuators B: Chem. 141 (2009) 511;
(b) R. Triboulet, J. Perriere, Epitaxial growth of ZnO films, Prog. Cryst. Growth Charact. 47 (2003) 65–138;
(c) M. Willander, O. Nur, Q.X. Zhao, L.L. Yang, M. Lorenz, B.Q. Cao, J. Zúñiga Pérez, C. Czekalla, G. Zimmermann, M. Grundmann, A. Bakin, A. Behrends, M. Al-Suleiman, A. El-Shaer, A. Che Mofor, B. Postels, A. Waag, N. Boukos, A. Travlos, H.S. Kwack, J. Guinard, D. Dang Le Si, Zinc oxide nanorod based photonic devices: recent progress in growth, light emitting diodes and lasers, Nanotechnology 20 (2009) 332001.
[7] Z.L. Wang, Nanodevice, nanosensors and nanocantilevers based on semiconducting oxide nanobelts, in: Z.L. Wang (Ed.), Nanowires and Nanobelts–materials, properties and devices. Vol. II. Nanowires and Nanobelts of Functional Materials, Kluwer Academic Publisher, 2003.

[8] (a) H.T. Wang, B.S. Kang, F. Ren, L.C. Tien, P.W. Sadik, D.P. Norton, S.J. Pearton, J. Lin, Detection of hydrogen at room temperature with catalyst-coated multiple ZnO nanorods, Appl. Phys. A 81 (2005) 1117;
(b) H.T. Wang, B.S. Kang, F. Ren, L.C. Tien, P.W. Sadik, D.P. Norton, S.J. Pearton, J. Lin, Hydrogen-selective sensing at room temperature with ZnO nanorods, Appl. Phys. Lett. 86 (2005) 243503.
[9] O. Lupan, G. Chai, L. Chow, Novel hydrogen gas sensor based on single ZnO nanorod, Microelectron. Eng. 85 (2008) 2220.
[10] O. Lupan, V.V. Ursaki, G. Chai, L. Chow, G.A. Emelchenko, I.M. Tiginyanu, A.N. Gruzintsev, A.N. Redkin, Selective hydrogen gas nanosensor using individual ZnO nanowire with fast response at room temperature, Sens. Actuators B: Chem. 144 (2010) 56.
[11] D.I. Suh, S.Y. Lee, T.H. Kim, J.M. Chun, E.K. Suh, O.B. Yang, S.K. Lee, The fabrication and characterization of dye-sensitized solar cells with a branched structure of ZnO nanowires, Chem. Phys. Lett. 442 (2007) 348–353.
[12] J.B. Baxter, E.S. Aydil, Dye-sensitized solar cells based on semiconductor morphologies with ZnO nanowires, Sol. Energy Mater. Sol. Cells 90 (2006) 607–622.
[13] Y. Xia, P. Yang, Y. Sun, Y. Wu, B. Mayers, B. Gates, Y. Yin, F. Kim, H. Yan, One-dimensional nanostructures: synthesis, characterization, and applications, Adv. Mater. 15 (2003) 353–389.
[14] T. Pauporté, Design of solution-grown ZnO nanostructures, in: Z.M. Wang (Ed.), Lecture Notes on Nanoscale Science and Technology. Volume 5. Toward Functional Nanomaterials, Springer Books, New York, 2009, pp. 77–125.
[15] Z.L. Wang, ZnO nanowire and nanobelt platform for nanotechnology, Mater. Sci. Eng. R 64 (2009) 33–71.
[16] M. Law, L.E. Greene, J.C. Johnson, R. Saykally, P. Yang, Nanowire dye-sensitized solar cells, Nat. Mater. 4 (2005) 455–459.
[17] Q.H. Li, Q. Wan, Y.X. Liang, T.H. Wang, Electronic transport through individual ZnO nanowires, Appl. Phys. Lett. 84 (2004) 4556.
[18] H. Kind, H. Yan, B. Messer, M. Law, P. Yang, Nanowire ultraviolet photodetectors and optical switches, Adv. Mater. (Weinheim, Ger.) 14 (2002) 158.
[19] C.H. Liu, W.C. Yiu, F.C.K. Au, J.X. Ding, C.S. Lee, S.T. Lee, Electrical properties of zinc oxide nanowires and intramolecular p–n junctions, Appl. Phys. Lett. 83 (2003) 3168.
[20] D.C. Reynolds, D.C. Look, B. Jogai, Optically pumped ultraviolet lasing from ZnO, Solid State Commun. 99 (1996) 873;
D.M. Bagnall, Y.F. Chen, Z. Zhu, T. Yao, S. Koyama, M.Y. Shen, T. Goto, Optically pumped lasing of ZnO at room temperature, Appl. Phys. Lett. 70 (1997) 2230.
[21] O. Lupan, T. Pauporté, B. Viana, Adv. Mater., under review.
[22] C.-H. Ku, J.-J. Wu, Chemical bath deposition of ZnO nanowire–nanoparticle composite electrodes for use in dye-sensitized solar cells, Nanotechnology 18 (2007) 505706.
[23] (a) M. Saito, S. Fujihara, Large photocurrent generation in dye-sensitized ZnO solar cells, Energy Environ. Sci. 1 (2008) 280–283;
(b) K. Keis, E. Magnusson, H. Lindstrom, S.E. Lindquist, A. Hagfeldt, A 5% efficient photoelectrochemical solar cell based on nanostructured ZnO electrodes, Sol. Energy Mater. Sol. Cells 73 (2002) 51.
[24] T. Yoshida, J. Zhang, D. Komatsu, S. Sawatani, H. Minoura, T. Pauporté, D. Lincot, T. Oekermann, D. Schlettwain, H. Tada, D. Wöhrle, K. Funabiki, M. Matsui, H. Miura, H. Yanagi, Electrodeposition of inorganic/organic hybrid thin films, advanced functional materials, Adv. Funct. Mater. 19 (2009) 17–43.
[25] J.B. Baxter, E.S. Aydil, Nanowire-based dye-sensitized solar cells, Appl. Phys. Lett. 86 (2005) 053114.
[26] A. Du Pasquier, H. Chen, Y. Lu, Dye sensitized solar cells using well-aligned zinc oxide nanotip arrays, Appl. Phys. Lett. 89 (2006) 253513.
[27] N. Kopidakis, N.R. Neale, K. Zhu, J. Van De Lagemaat, A.J. Frank, Spatial location of transport-limiting traps in TiO_2 nanoparticle films in dye-sensitized solar cells, Appl. Phys. Lett. 87 (2005) 202106.
[28] P.V. Kamat, Meeting the clean energy demand: nanostructure architectures for solar energy conversion, J. Phys. Chem. C 111 (7) (2007) 2834.
[29] Z.L. Wang, Zinc oxide nanostructures: growth, properties and applications, J Phys.: Condens. Matter 16 (2004) R829–R858.
[30] O. Lupan, L. Chow, G. Chai, B. Roldan, A. Naitabdi, A. Schulte, H. Heinrich, Nanofabrication and characterization of ZnO nanorod arrays and branched microrods by aqueous solution route and rapid thermal processing, Mater. Sci. Eng. B: Solid 145 (2007) 57.
[31] N. Wang, Y. Cai, R.Q. Zhang, Growth of nanowires, Mater. Sci. Eng. R 60 (2008) 1–51.
[32] T. Pauporté, G. Bataille, L. Joulaud, F.J. Vermersch, Well-aligned ZnO nanowire arrays prepared by seed-layer-free electrodeposition and their Cassie–Wenzel transition after hydrophobization, J. Phys. Chem. C 114 (1) (2010) 194.
[33] T. Pauporté, D. Lincot, B. Viana, F. Pellé, Toward laser emission of epitaxial nanorod arrays of ZnO grown by electrodeposition, Appl. Phys. Lett. 89 (2006) 233112.
[34] C. Badre, T. Pauporté, M. Turmine, D. Lincot, ZnO nanowire array film with super water repellent properties, Nanotechnology 18 (2007) 365705.
[35] M.H. Huang, Y.Y. Wu, H. Feick, N. Tran, E. Weber, P.D. Yang, Catalytic growth of zinc oxide nanowires by vapor transport, Adv. Mater. (Weinheim, Ger.) 13 (2001) 113.
[36] W.I. Park, D.H. Kim, S.W. Jung, G.C. Yi, Metalorganic vapor-phase epitaxial growth of vertically well-aligned ZnO nanorods, Appl. Phys. Lett. 80 (2002) 4232.
[37] (a) L. Chow, O. Lupan, H. Heinrich, G. Chai, Self-assembly of densely packed and aligned bilayer ZnO nanorod arrays, Appl. Phys. Lett. 94 (2009) 163105;
(b) O. Lupan, L. Chow, G. Chai, S. Park, A. Schulte, Electric field assisted assem-

bly of perpendicular oriented ZnO nanorods on Si substrate, in: Technical Proceedings of the 2008 NSTI Nanotechnology Conference and Trade Show, NSTI-Nanotech, Nanotechnology, vol. 1, 2008, p. 567.

[38] Y. Leprince-Wang, A. Yacoubi-Ouslim, G.Y. Wang, Structure study of electrodeposited ZnO nanowires, Microelectron. J. 36 (2005) 625–628.

[39] T. Pauporté, E. Jouanno, F. Pellé, B. Viana, P. Ashehoung, Key growth parameters for the electrodeposition of ZnO films with an intense UV-light emission at room temperature, J. Phys. Chem. C 113 (2009) 10422–10431.

[40] Q. Zhao, D. Wang, L. Peng, Y. Lin, M. Yang, T. Xie, Surface photovoltage study of photogenerated charges in ZnO nanorods array grown on ITO, Chem. Phys. Lett. 434 (2007) 96–100.

[41] Y. Su, L. Li, Y. Chen, Q. Zhou, M. Gao, Q. Chen, Y. Feng, The synthesis of Sn-doped ZnO nanowires on ITO substrate and their optical properties, J. Cryst. Growth 311 (2009) 2466–2469.

[42] Y.F. Hsu, Y.Y. Xi, A.B. Djurišić, W.K. Chan, ZnO nanorods for solar cells: hydrothermal growth versus vapor deposition, Appl. Phys. Lett. 92 (2008) 133507.

[43] R. Ghosh, D. Basak, S. Fujihara, Effect of substrate-induced strain on the structural, electrical, and optical properties of polycrystalline ZnO thin films, J. Appl. Phys. 96 (2004) 2689.

[44] X. Teng, H. Fan, S. Pan, C. Ye, G. Li, Abnormal photoluminescence of ZnO thin film on ITO glass, Mater. Lett. 61 (2007) 201–204.

[45] K. Keem, H. Kim, G.T. Kim, J.S. Lee, B. Min, K. Cho, M.Y. Sung, S. Kim, Photocurrent in ZnO nanowires grown from Au electrodes, Appl. Phys. Lett. 84 (2004) 4376.

[46] C.H. Yi, I. Yasui, Y. Shigesato, Oriented tin-doped indium oxide films on <0 0 1> preferred oriented polycrystalline ZnO films, Jpn. J. Appl. Phys. 34 (1995) 1639.

[47] X. Liu, Z. Jin, S. Bu, J. Zhao, Z. Liu, Effect of buffer layer on solution deposited ZnO films, Mater. Lett. 59 (2005) 3994–3999.

[48] O. Lupan, T. Pauporté, L. Chow, B. Viana, F. Pellé, L.K. Ono, B. Roldan Cuenya, H. Heinrich, Effects of annealing on properties of ZnO thin films prepared by electrochemical deposition in chloride medium, Appl. Surf. Sci. 256 (2010) 1895.

[49] A. Goux, T. Pauporté, D. Lincot, Oxygen reduction on zinc oxide electrodes in KCl aqueous solution at 70 °C, Electrochim. Acta 51 (2006) 3168–3172.

[50] T. Le Bahers, T. Pauporté, G. Scalmani, C. Adamo, I. Ciofini, A TD-DFT investigation of ground and excited state properties in indoline dyes used for dye-sensitized solar cells, Phys. Chem. Chem. Phys. 11 (2009) 11276–11284.

[51] N. Fujimura, T. Nishihara, S. Goto, J. Xu, T. Ito, Control of preferred orientation for ZnO$_x$ films: control of self-texture, J. Cryst. Growth 130 (1993) 269.

[52] R.J. Hong, J.D. Shao, H.B. He, Z.X. Fan, Effects of oxygen partial pressure on optical absorption edge and UV emission energy of ZnO films, Chin. Opt. Lett. 3 (2005) 428.

[53] T. Pauporté, O. Lupan, J. Cryst. Growth, under review.

[54] H. Hasebe, K. Kikushima, J. Chem. Soc. Jpn. 90 (1969) 112.

[55] J.M. Calleja, M. Cardona, Resonant Raman scattering in ZnO, Phys. Rev. B. 16 (1977) 3753.

[56] V.V. Ursaki, I.M. Tiginyanu, V.V. Zalamai, E.V. Rusu, G.A. Emelchenko, V.M. Masalov, E.N. Samarov, Multiphonon resonant Raman scattering in ZnO crystals and nanostructured layers, Phys. Rev. B 70 (2004) 155204.

[57] V.V. Zalamai, V.V. Ursaki, E.V. Rusu, P. Arabadji, I.M. Tiginyanu, L. Sirbu, Photoluminescence and resonant Raman scattering in highly conductive ZnO layers, Appl. Phys. Lett. 84 (2004) 5168.

[58] V.V. Ursaki, O.I. Lupan, L. Chow, I.M. Tiginyanu, V.V. Zalamai, Rapid thermal annealing induced change of the mechanism of multiphonon resonant Raman scattering from ZnO nanorods, Solid State Commun. 143 (2007) 437.

[59] E. Iliopoulos, D. Doppalopudi, H.M. Ng, T.D. Moustakas, Broadening of near-band-gap photoluminescence in n-GaN films, Appl. Phys. Lett. 73 (1998) 375.

[60] T.N. Morgan, Broadening of impurity bands in heavily doped semiconductors, Phys. Rev. 139 (1965) A343.

[61] S.B. Zhang, S.-H. Wei, A. Zunger, Intrinsic n-type versus p-type doping asymmetry and the defect physics of ZnO, Phys. Rev. B 63 (2001) 075205.

[62] E. Oba, S.R. Nishitani, S. Isotani, H. Adachi, I. Tanaka, Energetics of native defects in ZnO, J. Appl. Phys. 90 (2001) 824.

[63] M. Guo, P. Diao, X.D. Wang, S.M. Cai, The effect of hydrothermal growth temperature on preparation and photoelectrochemical performance of ZnO nanorod array films, J. Solid State Chem. 178 (2005) 3210.

[64] N.O.V. Plank, I. Howard, A. Rao, M.W.B. Wilson, C. Ducati, R.S. Mane, J.S. Bendall, R.R.M. Louca, N.C. Greenham, H. Miura, R.H. Friend, H.J. Snaith, M.E. Welland, Efficient ZnO nanowire solid-state dye-sensitized solar cells using organic dyes and core–shell nanostructures, J. Phys. Chem. C 113 (2009) 18515–18522.

[65] C.H. Ku, J.J. Wu, Electron transport properties in ZnO nanowire array/ nanoparticle composite dye-sensitized solar cells, Appl. Phys. Lett. 91 (2007) 093117.

[66] C.Y. Jiang, X.W. Sun, G.Q. Lo, D.L. Kwong, J.X. Wang, Improved dye-sensitized solar cells with a ZnO-nanoflower photoanode, Appl. Phys. Lett. 90 (2007) 263501.

[67] J.B. Baxter, A.M. Walker, K. van Ommering, E.S. Aydil, Synthesis and characterization of ZnO nanowires and their integration into dye-sensitized solar cells, Nanotechnology 17 (2006) S304–S312.

[68] H. Gao, G. Fang, M. Wang, N. Liu, L. Yuan, C. Li, L. Ai, J. Zhang, C. Zhou, S. Wu, X. Zhao, The effect of growth conditions on the properties of ZnO nanorod dye-sensitized solar cells, Mater. Res. Bull. 43 (2008) 3345–3351.

[69] C.H. Ku, J.J. Wu, Chemical bath deposition of ZnO nanowire–nanoparticle composite electrodes for use in dye-sensitized solar cells, Nanotechnology 18 (50) (2007) 505706.